Journal of Materials Science: Materials in Electronics
https://doi.org/10.1007/s10854-020-03532-2

Structural and magnetic properties of rare-earth-free MnAl(MCNT)/Fe nanocomposite magnets processed by resin-bonding technique

P. Saravanan[1] · Sarah Saju[1] · V. T. P. Vinod[2] · Miroslav Černík[2]

Received: 11 March 2020 / Accepted: 1 May 2020

Abstract
In this study, the potential of multi-walled carbon nanotubes (MCNT) in processing rare-earth-free MnAl(MCNT)/Fe nanocomposite magnets was exploited through adopting a combination of surfactant-assisted milling and resin-bonding techniques. The required hard and soft magnetic phases such as MnAl(MCNT) and α-Fe, respectively, were individually subjected to surfactant-assisted high-energy ball milling. The surfactant-coated MnAl(MCNT) and Fe nanopowders, thus, obtained were characterized with respect to their structural and magnetic properties. Relatively, a very high coercivity, H_c (4.48 kOe), was obtained for the surfactant-coated MnAl(MCNT) powders after 6 h of milling, while in the case of Fe powders with high saturation magnetization, M_s (218.6 emu/g) was achieved at 3 h of surfactant-assisted milling. The MnAl(MCNT) powders with high H_c were mixed with the Fe powders of high M_s with different weight percentages: 0, 5 and 10. The nanocomposite powder mixtures were further milled for 1 h and then processed in the form of resin bonded magnets under aligning magnetic field of 20 kOe. The obtained bonded nanocomposite magnet, i.e. MnAl(MCNT) with 5 wt% of Fe addition demonstrated a good combination of high M_s (63.7 emu/g) and high H_c (4.46 kOe).

1 Introduction

In recent years, increasing attention has been paid towards enhancing the performance of high-energy rare earth (RE) permanent magnets (PM) through adopting novel and high-throughput methods [1–3]. Nevertheless, because of limited availability of RE elements such as Nd, Dy and Sm in the worldwide scale, it is important to develop new kind of PM materials free from RE elements. In this context, the processing of RE-free PMs has gained widespread attention towards sustainable energy [4–6]. Among the various RE-free PMs, the magnetic performance of MnAl-based alloys lies in between the RE magnets and AlNiCo. More particularly, the MnAl alloy system with ferromagnetic (FM) $L1_0$ phase (P4/mmm, AuCu I type, known as τ-phase) exhibits maximum magnetic energy density product per unit mass, relative to the conventional PMs [7, 8]. However, a critical process concern is that the τ-phase of Mn–Al alloy is metastable and hence a small addition of carbon (2–3 at.%) is often preferred for stabilization of τ-phase [9]. Other than the carbon addition, the τ-phase stabilization in Mn–Al alloy has also been attempted with the other doping elements such as boron, copper and zirconium [10, 11].

Until now, many investigations have been made to process the Mn–Al- and/or Mn–Al–C-based alloys using ball milling and melt spinning techniques in the form of nanopowders and ribbons, respectively, with isotropic characteristics [9–13]; however, the obtained coercivity (H_c) and saturation magnetization (M_s) values are not comparable with their theoretical limits [14]. Any enhancement in these magnetic parameters could be possible by adopting new processing strategies and doping elements for the Mn–Al alloys. In this context, we, herein, propose (i) to replace the conventional doping element (carbon) with multi-walled carbon nanotubes (MCNT) while melting the Mn–Al alloy and (ii) to implement the concept of exchange-coupled nanocomposite magnets for the MCNT-modified Mn–Al alloy. Of course, the following characteristics of MCNTs make them as a valuable elemental addition for the Mn–Al alloy system. The

✉ P. Saravanan
psdrdo@gmail.com; ps@dmrl.drdo.in

✉ Miroslav Černík
miroslav.cernik@tul.cz

[1] Defence Metallurgical Research Laboratory, Hyderabad 500058, India

[2] Department of Natural Sciences, Institute for Nanomaterials, Advanced Technologies and Innovation, Technical University of Liberec, Studentská 1402/2, 461 17 Liberec 1, Czech Republic

Published online: 10 May 2020

MCNTs not only exhibit properties quite similar to that of metals, but also are well-known for their strong encapsulation and application as nanoscaled magnetic objects during the processing of metal–matrix composites [15, 16]. In particular, when compared to the other forms of carbon nanomaterials, MCNTs exhibit distinct FM properties. Besides, the addition of MCNTs can impede the motion of domain walls during the magnetization reversal and thereby enhance the H_c of parent Mn–Al alloy [17].

In general, for producing the exchange-coupled nanocomposite magnets, hard magnetic phases such as $Nd_2Fe_{14}B$ and $SmCo_5$ type of RE magnetic material and a soft magnetic phase of Co or α-Fe are more often preferred [18, 19]. In this study, to process the MnAl(MCNT) hard magnetic phase in the form of exchange-coupled nanocomposite magnet, α-Fe was chosen as a soft magnetic phase. This is because, α-Fe exhibits large magnetic moment and is abundant and relatively cheap when compared to the other FM elements such as Ni and Co. As far as the synthesis strategies are concerned for the exchange-coupled nanocomposite magnets, soft-chemical methods [19], electroless coating [20] and surfactant-assisted milling [21] were found to be more promising. The grain size values achieved in these methods were relatively smaller as compared to the conventional milling, and thereby, a strong exchange-coupling between the hard and soft magnetic phases can be established.

For our hard (MnAl(MCNT))/soft (α-Fe) magnetic nanocomposites, the surfactant-assisted ball milling has been adopted, as this technique is capable of producing nanocrystalline flakes in large quantities [22, 23]. The MnAl(MCNT)/Fe composite flakes, thus, obtained were consolidated in the form of bulk magnets using resin-bonding technique under aligning magnetic field. The resultant bonded composite magnets demonstrated a good combination of both hard and soft magnetic properties such as high H_c and high M_s, respectively, with crystallographically anisotropic characteristics. The MnAl(MCNT)/Fe bonded magnets such as those processed in this study possess many advantages over the conventional sintered magnets, such as low cost and excellent availability of Mn, Al and Fe materials, good machinability, excellent corrosion resistance and weight reduction. These properties make them as a potential candidate for various technological applications, such as power electronics, motors, magnetic rollers for copier and laser printer and magnetic rings for aerodynamic component and automotive parts.

2 Materials and methods

Mn55Al44(MCNT) alloy was arc-melted using high-purity (> 99.5%) constituent metal elements such as Mn and Al and MCNT powders in appropriate amounts under argon atmosphere. Since the vapour pressure of Mn is high, it undergoes some amount of evaporation losses during arc melting. To estimate this loss, a few trail melting experiments were conducted for the Mn54Al46 alloy and the deviation in the initial and final composition was estimated. Based on the composition deviation, excess amount of Mn (~ 2 wt%) was added with respect to the actual Mn content. By this means, the required composition was attained in the MnAl alloy ingots. MCNTs having diameters varying from 15 to 40 nm and lengths of several tens of microns were used. More details on the structural and magnetic properties of MCNTs can be found elsewhere [17]. Further, it should be noted that the best magnetic properties for the MnAl alloy were obtained for a carbon content just above the solubility of carbon atoms (slightly above 1 at.%) [14]. For similar reasons, the amount of MCNT was preferred as 1 at.%. The arc-melted MnAl(MCNT) alloy was crushed and sewed to obtain powder particles < 300 μm and then they were subjected to high-energy milling using a planetary ball mill (FRITSCH pulverisette). Both milling vials and balls were made up of tungsten carbide and a milling speed of 200 rpm was maintained. For a planetary type of high-energy ball milling, a ball to crushed powder ratio of 10:1 is most commonly used in order to have significant grain refinement [24]; accordingly, this ratio was chosen in this study. A mixture containing 1:1 ratio of oleic acid and oleylamine was used as surfactant along with the solvent: *n*-heptane. The amount of surfactant was about 10 wt. % of the crushed powder dispersed in the solvent and this amount is good enough to produce nanocrystalline flakes [25]. As similar to the processing of hard magnetic phase, MnAl(MCNT), the soft magnetic phase, i.e. α-Fe powders, was individually processed via surfactant-assisted milling. The elemental composition and grain morphology of the alloy ingots and their milled counterpart powders were performed by energy

dispersive X-ray (EDX) analysis attached with a scanning electron microscope (SEM, Leo 440i). Powder X-ray diffraction (XRD) measurements were carried out using a Rigaku Smartlab Multipurpose diffractometer system with Co–K_α radiation. The magnetic properties were evaluated at room temperature using a vibrating sample magnetometer (VSM) up to a maximum field of 20 kOe (2 T).

3 Results and discussion

The cross-sectional microstructure of MnAl(MCNT) alloy ingot is depicted in Fig. 1a, which reveals a two-phase microstructure. The line scan profile (marked in Fig. 1a) indicates that the concentration of Mn drastically decreases over a distance of 30 nm on each side of the interface between the two distinct phases (Fig. 1b). The two phases were identified as τ-MnAl and β-Mn (Mn-rich) from the XRD analysis (Fig. 1c). The estimated elemental composition was in close agreement against the starting Mn55Al44(MCNT) composition with an error contribution of ± 3.2%. The magnetic parameters such as H_c (900 Oe) and M_s (63.5 emu/g) values for the as-cast MnAl(MCNT) alloy were determined from the magnetic hysteresis loop (Fig. 1d) and these values apparently confirm the typical characteristics of a hard magnetic phase.

In Fig. 2, we show the SEM micrographs of 6 h milled MnAl(MCNT) powders without and with surfactant.

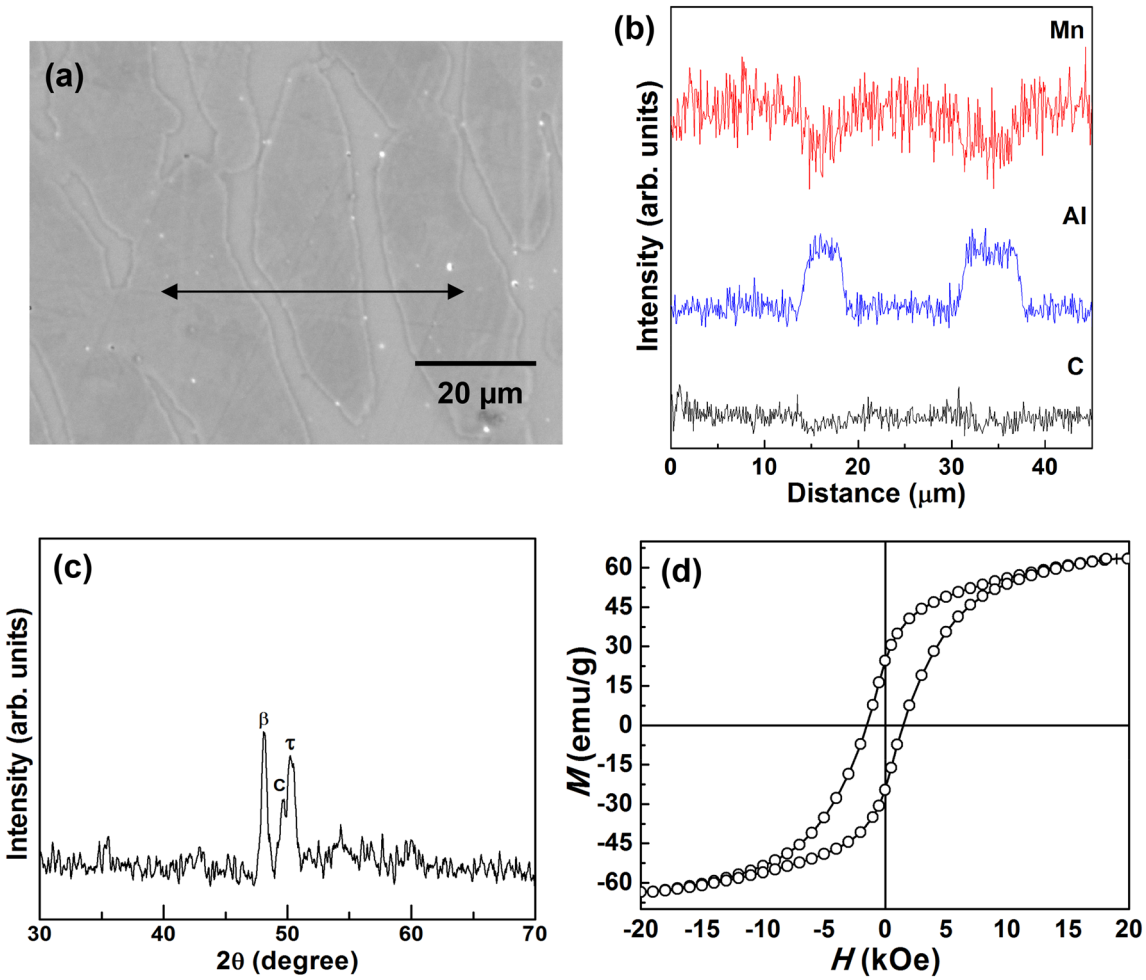

Fig. 1 Back-scattered SEM micrograph showing two-phase morphology for the as-cast MnAl(MCNT) alloy with the solid line marks in the region for EDS line scan (**a**) and its corresponding EDS profile (**b**). Typical XRD pattern (**c**) and M–H curve of the as-cast MnAl(MCNT) alloy ingot (**d**)

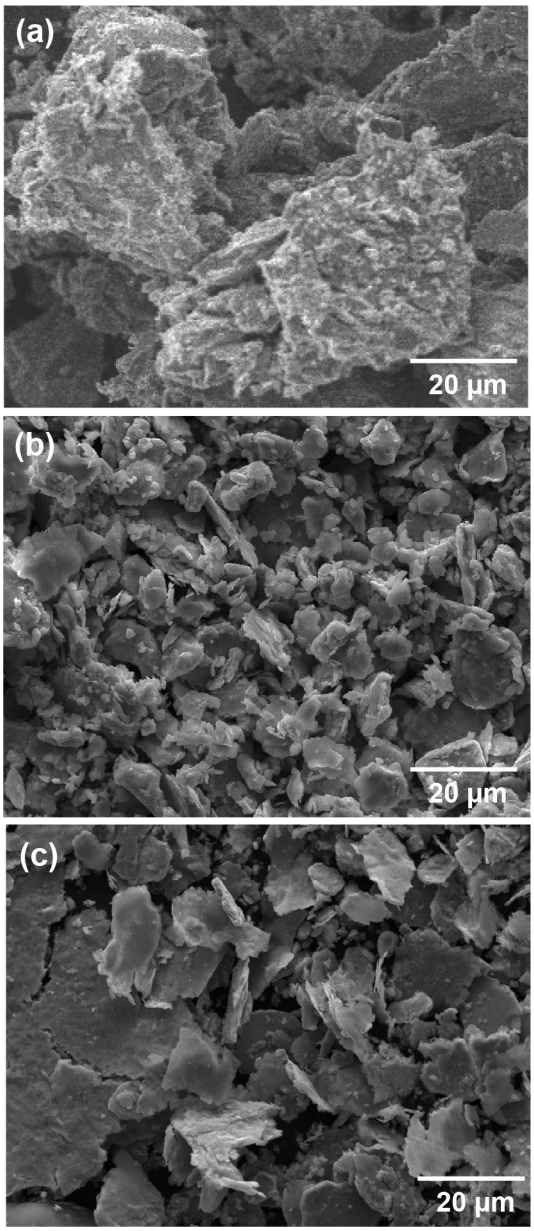

Fig. 2 SEM micrographs of crushed MnAl(MCNT) alloy ingots (**a**) and after being subjected to 6 h of milling without (**b**) and with surfactant (**c**)

The powders milled without surfactant revealed irregular morphology with a particle size distribution varying from 1 to 32 μm, whereas the powders processed with the surfactant-assisted milling showed the presence of fine particles with sizes ranging from 1 to 14 μm. Apart from the reduction in particle size, it is interesting to note that flake-like structures were obtained for the surfactant-coated MnAl(MCNT) powders (Fig. 2b). The possible mechanism for the evolution of such morphology during surfactant-assisted milling has been previously elucidated by Cui et al. and Saravanan et al. in the case of $SmCo_5$ [22] and Mn–Al [23] alloy systems, respectively. According to them, the irregular particles formed during milling fail by cleavage along the easy glide basal plane without an appreciable increase in the density of crystal defects. This is followed by continuation of cleavage along the parallel basal planes via layer-by-layer splitting to form nanocrystalline flakes. The surfactant adsorbed by the fresh surface of flakes prevents their cold welding and hence their agglomeration. For the 6 h milled surfactant-coated MnAl(MCNT) powders, the thickness and lengths of flakes were estimated in the range of 30–3000 nm and 1–75 μm, respectively, with aspect ratios as high as 10^2 to 10^3. The XRD patterns for the MnAl(MCNT) powders processed without and with surfactant are presented in Fig. 3a and b, respectively. The XRD patterns are almost similar and the evolution of τ- and β-phases with some traces of carbon are evident in both cases. For the powders milled without surfactant, the intensity of τ-phase is found to be decreased with increase of milling time. In contrast, the intensities of both τ- and β-phases are preserved in the case of surfactant-coated MnAl(MCNT) powders.

The magnetic hysteresis loops for the milled MnAl(MCNT) powders without and with surfactant are shown in Fig. 4a and b, respectively. The shapes of the *M–H* curves are entirely different in both cases. For the MnAl(MCNT) powders processed without surfactant, a significant drop in the M_s value from 63.5 (0 h) to 20.5 emu/g (6 h) can be noticed, whereas in the case of surfactant-coated powders, the reduction in M_s values are minimal (from 63.5 to 54.7 emu/g). A plausible reason for the decreased M_s values can be attributed to the reduction in τ-phase content and/or site disorder induced by the high-energy milling process [26]. This effect seems to be more pronounced in the case of powders processed without surfactant (Fig. 3a) and hence they showed a large reduction in the M_s value after 6 h of milling. In contrast, the estimated H_c values established an increasing trend against the milling time in both cases and this trend can be explained by the dependence of coercivity

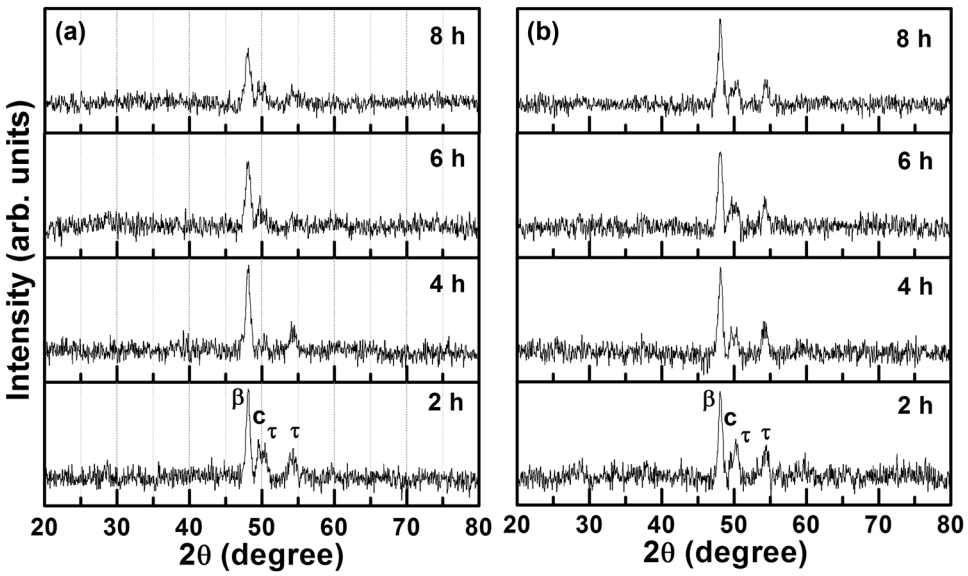

Fig. 3 X-ray diffraction patterns obtained for the MnAl(MCNT) powders as a function of milling time. Milling performed without (**a**) and with surfactant (**b**)

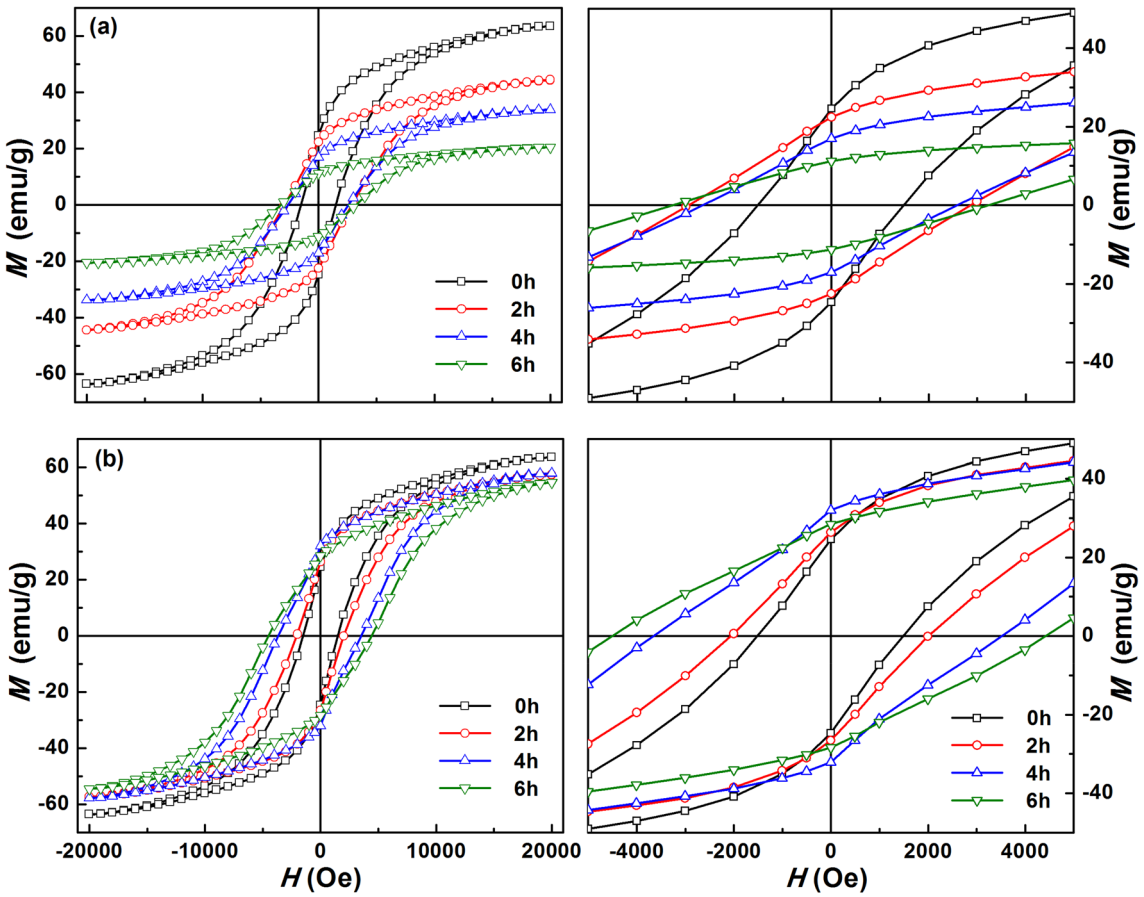

Fig. 4 Magnetic hysteresis curves for the MnAl(MCNT) powders obtained at different milling intervals without (**a**) and with surfactant (**b**). The corresponding enlarged views are provided on the right side

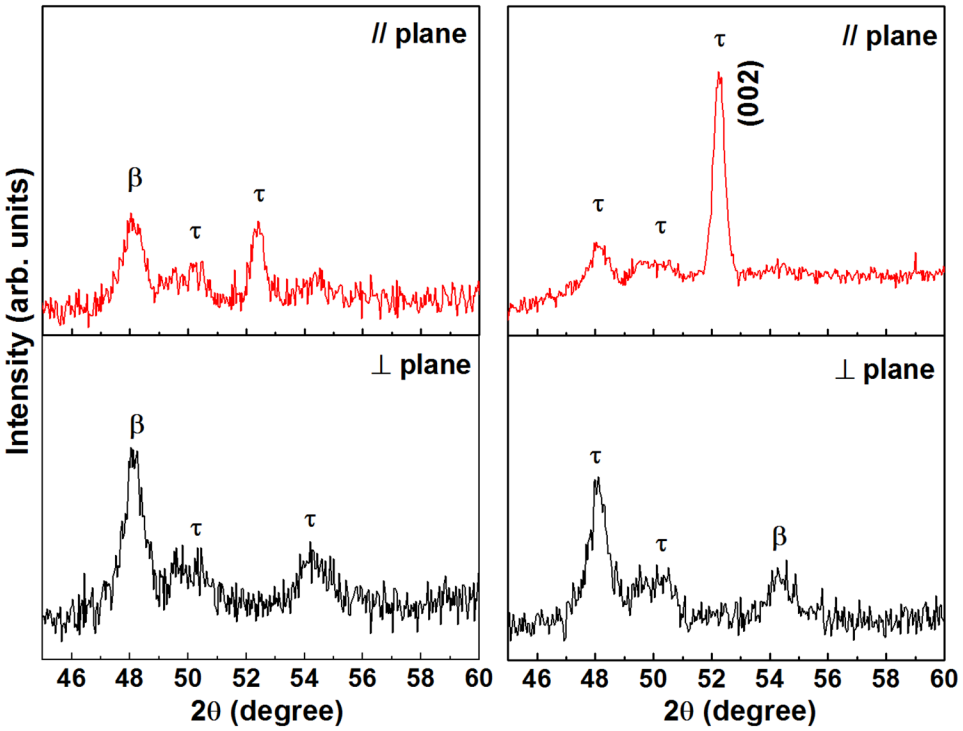

Fig. 5 XRD patterns of MnAl(MCNT) resin bonded magnets processed under aligning magnetic field. Powders milled without (**a**) and with surfactant (**b**). The intensity of (0 0 2) diffraction peak is the measure of texture or the c-axis alignment of τ-phase

on the grain size [27, 28]. Maximum H_c values of 3.24 and 4.46 kOe were obtained for the 6 h milled MnAl(MCNT) powders processed without and with surfactant, respectively.

The anisotropy characteristics of 6 h milled MnAl(MCNT) powders were studied by processing them into polymer bonded magnets. While curing the polymer (epoxy), a homogenous magnetic field of 2 T was applied in order to induce grain orientation. The XRD patterns of the aligned MnAl(MCNT) magnets processed from the bare and surfactant-coated powders are shown in Fig. 5a and b, respectively. In the case of bonded magnets processed from the bare MnAl(MCNT) powders, the intensities of the characteristic peaks are found to be almost the same in the directions parallel and perpendicular to the alignment (Fig. 5a), whereas the bonded magnets made out of the surfactant-coated powders showed intense peaks for the characteristic τ-phase, with a distinct parallel and perpendicular plane texture (Fig. 5b). In the case of $L1_0$ Mn–Al, the intensity of (0 0 2) peak can be considered as a measure of *c*-axis alignment (texture) and the degree of texturing for this peak [29], i.e. in terms of texture coefficient was calculated as 1.26 in the perpendicular plane. This apparently indicates the evolution of possible texture for the τ-phase during epoxy curing.

The surface morphologies of starting Fe powders and their milled counterparts without and with surfactant are depicted in Fig. 6. It can be noticed that upon milling, the spherical morphology of starting powders (Fig. 6a) is found to be transformed into platelet shapes in both cases (Fig. 6b and c) and this is mainly attributed to the ductile nature of Fe [30, 31]. In the case of surfactant-coated Fe powders, the thickness of platelet appears to be relatively low. The measured M–H loops for the milled Fe powders without and with surfactant are shown in Fig. 7a and b, respectively. The estimated M_s values demonstrated an increasing trend at

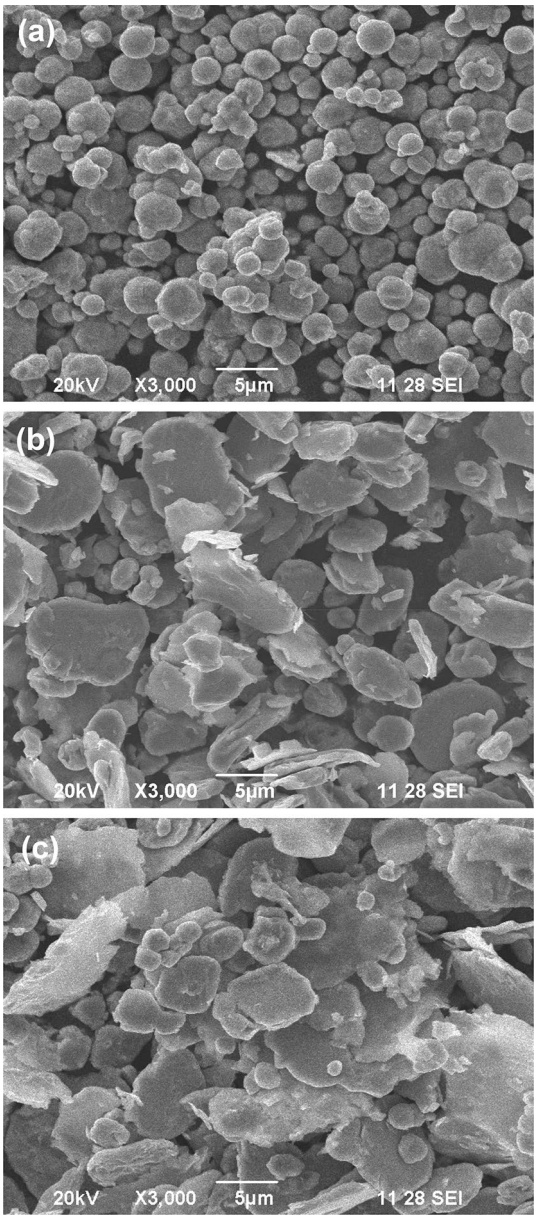

Fig. 6 SEM micrographs of starting Fe powders (**a**) and after being subjected to 6 h of milling without (**b**) and with surfactant (**c**)

early milling hours, followed by a decreasing trend at larger milling duration. For the surfactant-coated Fe powders, the M_s value attained a maximum (218.6 emu/g) at early milling hours (3 h), whereas in the case of bare Fe powders, a maximum M_s value of 213.3 emu/g was obtained at 5 h of milling.

For the processing of MnAl(MCNT)/Fe bonded magnets, the surfactant-coated powders that possess high H_c (6 h milled MnAl(MCNT)) and high M_s (3 h milled Fe) were considered. In the case of uncoated powders, 5 h milled Fe was chosen, as they showed a high M_s value. The addition of soft phase (Fe) was maintained as 5 and 10 wt% with respect to the hard phase content: MnAl(MCNT). The nanocomposite powder mixture, thus, obtained was mixed thoroughly and then subjected to milling for 1 h for attaining homogeneity. Prior to the epoxy bonding, the elemental composition of the milled nanocomposite powders was studied using EDX analysis and the obtained results are given in Table 1. The magnetic hysteresis loops for the MnAl(MCNT) + x wt% Fe ($x = 0$, 5 and 10) bonded nanocomposite magnets are shown in Fig. 8. The bonded magnets processsed with the uncoated MnAl(MCNT)/Fe powders showed no significant improvement in their magnetic properties; rather they exhibited the effect of decoupling upon adding the Fe phase (Fig. 8a). On the contrary, the bulk magnets obtained from the surfactant-coated MnAl(MCNT)/Fe powders revealed smooth hysteresis loops. The measured M_s value is found to be increased from 55.8 to 74.4 emu/g upon adding 10 wt% Fe, while the H_c value has decreased from 4.5 to 3.6 kOe. With the addition of 5 wt% Fe, the H_c values are almost retained with respect to that of those obtained for the 6 h milled MnAl(MCNT) powders, while the M_s value has increased to 63.7 emu/g. This sort of behaviour apparently suggests the existence of strong exchange-coupling between the MnAl(MCNT) and Fe magnetic phases. The M_s and H_c values such as those obtained for the bulk nanocomposite magnets are relatively higher when compared to the previously reported values [32].

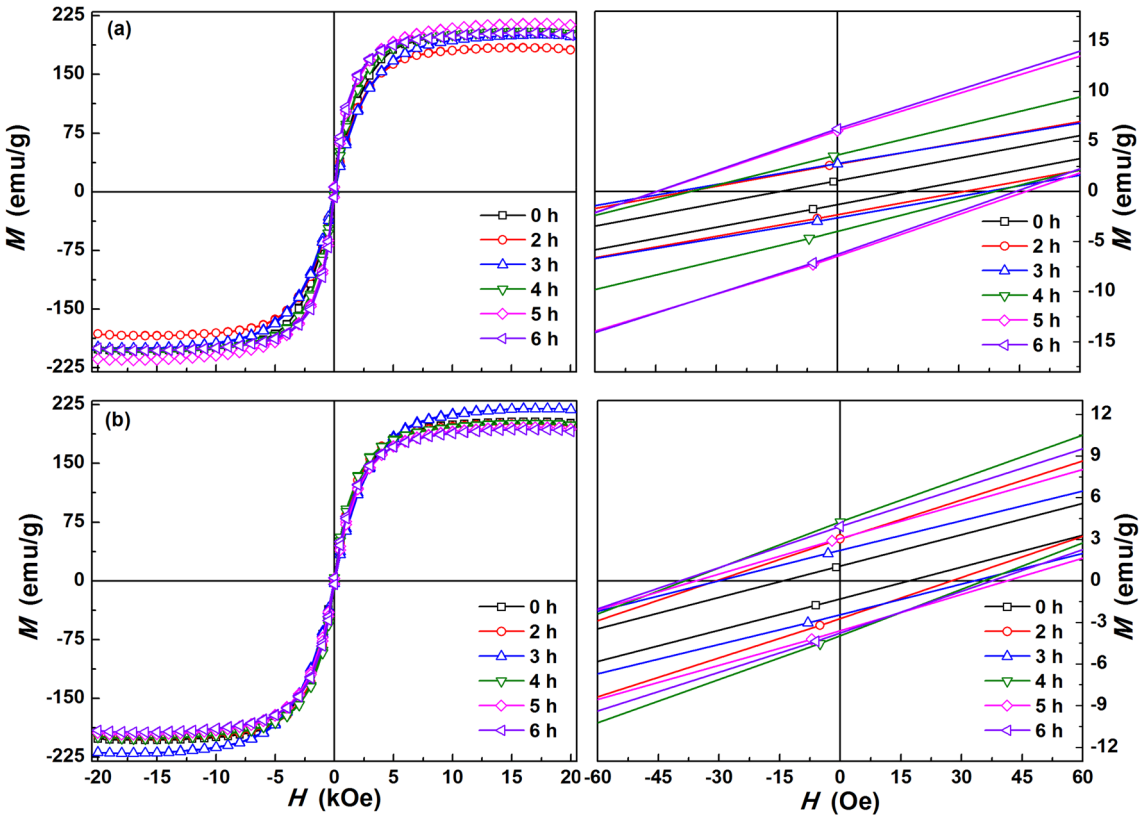

Fig. 7 Magnetic hysteresis curves for the Fe powders obtained at different milling intervals without (**a**) and with surfactant (**b**). The corresponding enlarged views are provided on the right side

Table 1 Elemental composition of the 6 h milled MnAl(MCNT) alloy and their nanocomposite derivatives

Samples	Elemental composition (wt%)	
	Milled without surfactant	Milled with surfactant
MnAl(MCNT)	Mn: 53.82; Al:45.29; C: 0.89	Mn: 53.99; Al:45.08; C: 0.93
MnAl(MCNT) + 5 wt% Fe	Mn: 51.13; Al:43.15; C: 0.85 Fe: 4.87	Mn: 51.36; Al: 42.94; C: 0.89 Fe: 4.81
MnAl(MCNT) + 10 wt% Fe	Mn: 48.62; Al:40.71; C: 0.82 Fe: 9.85	Mn: 48.81; Al:40.54; C: 0.86 Fe: 9.79

4 Conclusion

The processing of RE-free nanocomposite magnets such as MnAl(MCNT)/Fe was successfully accomplished by taking the advantages of Mn55Al44(MCNT) and α-Fe as the hard and soft magnetic phases, respectively. High-energy milling (without and with surfactant) was employed to process the MnAl(MCNT) and Fe magnetic phases into fine powders and these powders were consolidated into bulk nanocomposite magnets using the resin-bonding process. The MnAl(MCNT) + 5 wt% Fe bonded nanocomposite magnets processed with the surfactant-coated powders, exhibited a significant improvement in the magnetic parameters such as M_s and H_c. The process strategies such as those adopted in this study provide a pathway for RE-free nanocomposite magnets using MnAl(MCNT) as a hard magnetic phase.

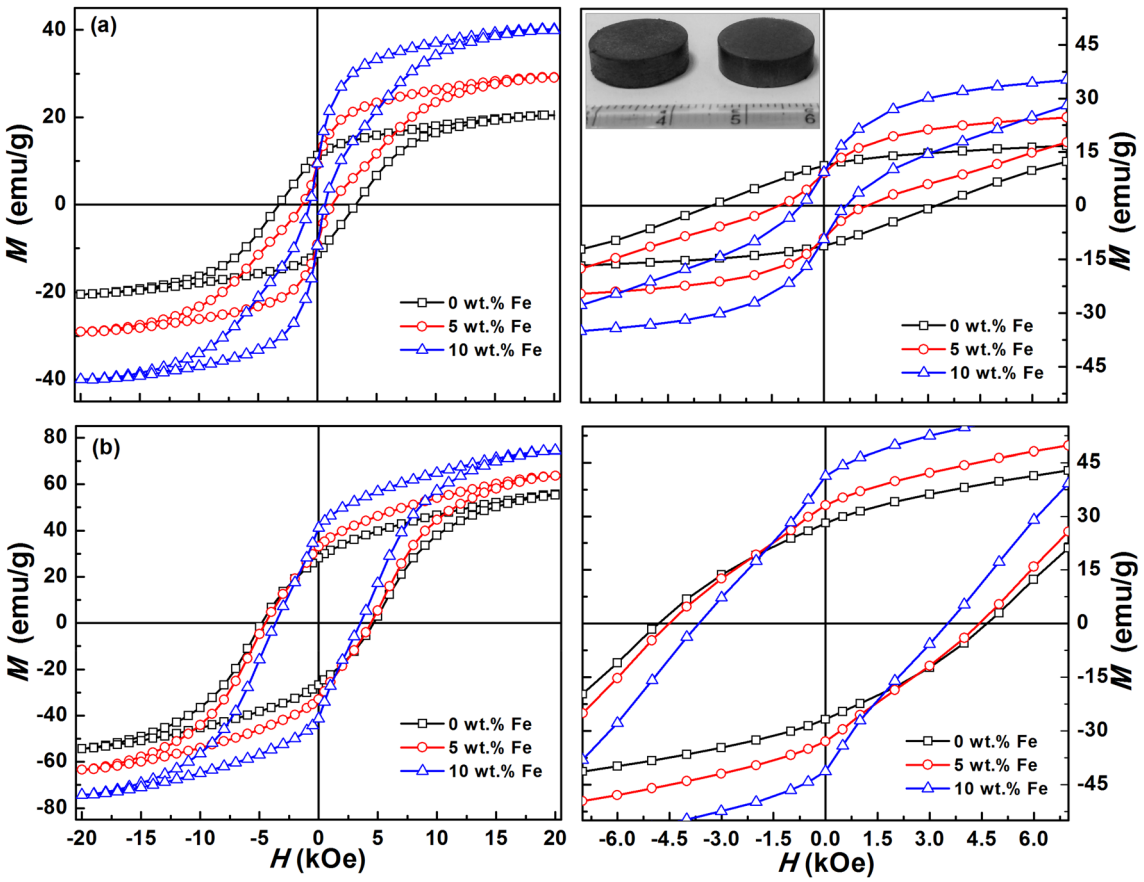

Fig. 8 Magnetic hysteresis curves for the MnAl(MCNT) + Fe (*x* wt%) nanocomposite magnets processed with the uncoated (**a**) and surfactant-coated powders (**b**). The corresponding enlarged views are provided on the right side. Inset shows a photograph of MnAl(MCNT)/Fe bonded nanocomposite magnet

Acknowledgements The financial support for the present study was extended by Defence Research and Development Organization, New Delhi, India. The authors VTPV and MC acknowledge the assistance provided by the Research Infrastructure NanoEnviCz, under Project No. LM2018124, supported by the Ministry of Education, Youth and Sports of the Czech Republic and the European Union – European Structural and Investment Funds in the frames of Operational Program Research, Development and Education—Project Hybrid Materials for Hierarchical Structures (HyHi, Reg. No. CZ.02.1.01/0.0/0.0/16_019/0000843).

References

1. J. Lee, T.-Y. Hwang, H.-B. Cho, J. Kim, Y.-H. Choa, Near theoretical ultra-high magnetic performance of rare-earth nanomagnets via the synergetic combination of calcium-reduction and chemoselective dissolution. Sci. Rep. **8**, 15656 (2018). https://doi.org/10.1038/s41598-018-33973-z
2. W.-L. Zuo, X. Zhao, T.-Y. Zhao, F.-X. Hu, J.-R. Sun, B.-G. Shen, Ultrathin $SmCo_5$ nanoflakes with high-coercivity prepared by solid particle (NaCl) and surfactant co-assisted ball milling. Sci. Rep. **6**, 25805 (2016). https://doi.org/10.1038/srep25805
3. Z. Zhang, X. Song, Y. Qiao, W. Xu, J. Zhang, M. Seyring, M. Rettenmayr, A nanocrystalline Sm–Co compound for high temperature permanent magnets. Nanoscale **5**, 2279–2284 (2013). https://doi.org/10.1039/C3NR34134H
4. J. Cui, M. Kramer, L. Zhou, F. Liu, A. Gabay, G. Hadjipanayis, B. Balasubramanian, D. Sellmyer, Current progress and future challenges in rare-earth-free permanent magnets. Acta Mater. **158**, 118–137 (2018). https://doi.org/10.1016/j.actamat.2018.07.049
5. D. Lia, Y. Lia, D. Pan, Z. Zhang, C.-J. Choi, Prospect and status of iron-based rare-earth-free permanent magnetic materials. J. Magn. Magn. Mater. **469**, 535–544 (2019). https://doi.org/10.1016/j.jmmm.2018.09.032
6. F. Ronning, S. Bader, Rare earth replacement magnets. J. Phys. **26**, 060301 (2014). https://doi.org/10.1088/0953-8984/26/6/060301
7. K. Patel, J. Zhang, S. Ren, Rare-earth-free high energy product manganese based magnetic materials. Nanoscale **10**, 11701–11718 (2018). https://doi.org/10.1039/C8NR01847B
8. J.M.D. Coey, New permanent magnets; manganese compounds. J. Phys. Condens. Matter **26**, 064211 (2014). https://doi.org/10.1088/0953-8984/26/6/064211
9. T. Ohtani, N. Kato, S. Kojima, Y. Sakamoto, I. Konno, M. Tsukamara, T. Kubo, Magnetic properties of Mn-Al-C permanent magnet alloys. IEEE Trans. Magn. **13**, 1328–1330 (1977). https://doi.org/10.1109/TMAG.1977.1059574
10. Z.W. Liu, C. Chen, Z.G. Zheng, B.H. Tan, R.V. Ramanujan, Phase transitions and hard magnetic properties for rapidly solidified

MnAl alloys doped with C, B, and rare earth elements. J. Mater. Sci. **47**, 2333–2338 (2012). https://doi.org/10.1007/s10853-011-6049-8
11. Y. Geng, M.J. Lucis, P. Rasmussen, J.E. Shield, Phase transformation and magnetic properties of rapidly solidified Mn–Al–C alloys modified with Zr. J. Appl. Phys. **118**, 033905 (2015). https://doi.org/10.1063/1.4927289
12. H. Fang, S. Kontos, J. Ångström, J. Cedervall, P. Svedlindh, K. Gunnarsson, M. Sahlberg, Directly obtained τ-phase MnAl, a high performance magnetic material for permanent magnets. J. Solid State Chem. **237**, 300–306 (2016). https://doi.org/10.1016/j.jssc.2016.02.031
13. Z. Xiang, C. Xu, T. Wang, Y. Song, H. Yang, W. Lub, Enhanced magnetization and energy product in isotropic nanocrystalline Mn55Al45 alloys with boron doping. Intermetallics **101**, 13–17 (2018). https://doi.org/10.1016/j.intermet.2018.07.003
14. Q. Zeng, I. Baker, J.B. Cui, Z.C. Yan, Structural and magnetic properties of nanostructured Mn–Al–C magnetic materials. J. Magn. Magn. Mater. **308**, 214–226 (2007)
15. R. Arvidsson, B.A. Sandén, Carbon nanomaterials as potential substitutes for scarce metals. J. Clean. Prod. **156**, 253–261 (2017). https://doi.org/10.1016/j.jclepro.2017.04.048
16. A. Azarniya, M.S. Safavi, S. Soviz, A. Azarniya, B. Chen, H.R.M. Hosseini, S. Ramakrishna, Metallurgical challenges in carbon nanotube-reinforced metal matrix nanocomposites. Metals **7**, 384 (2017). https://doi.org/10.3390/met7100384
17. P. Saravanan, J.H. Hsu, V.T. Vinod, M. Černík, S.V. Kamat, MWCNT reinforced τ-Mn–Al nanocomposite magnets through spark plasma sintering. J. Alloys Compd. **695**, 364–371 (2017). https://doi.org/10.1016/j.jallcom.2016.10.184
18. R. Skomski, J.M.D. Coey, Giant energy product in nanostructured two-phase magnets. Phys. Rev. B **48**, 15812–15816 (1993). https://doi.org/10.1103/PhysRevB.48.15812
19. Z. Ma, T. Zhang, C. Jiang, Exchange-coupled $SmCo_5$/Co nanocomposites synthesized by a novel strategy. RSC Adv. **5**, 89128–89132 (2015). https://doi.org/10.1039/C5RA15079E
20. N. Poudyal, K. Gandha, K. Elkins, J.P. Liu, Anisotropic $SmCo_5$/FeCo core/shell nanocomposite chips prepared via electroless coating. AIMS Mater. Sci. **2**, 294–302 (2015). https://doi.org/10.3934/matersci.2015.3.294
21. P. Saravanan, R. Gopalan, N.R. Rao, M.M. Raja, V. Chandrasekaran, $SmCo_5$/Fe nanocomposite magnetic powders processed by magnetic field-assisted ball milling with and without surfactant. J. Phys. D **40**, 5021–5026 (2007). https://doi.org/10.1088/0022-3727/40/17/002
22. B.Z. Cui, W.F. Li, G.C. Hadjipanayis, Formation of $SmCo_5$ single-crystal submicron flakes and textured polycrystalline nanoflakes. Acta Mater. **59**, 563–571 (2011). https://doi.org/10.1016/j.actamat.2010.09.060
23. P. Saravanan, D. Deepika, J.H. Hsu, V.T. Vinod, M. Černík, S.V. Kamat, A surfactant-assisted high energy ball milling technique to produce colloidal nanoparticles and nanocrystalline flakes in Mn–Al alloys. RSC Adv. **5**, 92406–92417 (2015). https://doi.org/10.1039/C5RA16550D
24. R.K. Gupta, B.S. Murty, N. Birbilis, *An overview of high-energy ball milled nanocrystalline aluminium alloys* (Springer, Berlin, 2017). https://doi.org/10.1007/978-3-319-57031-0
25. L. Zheng, B. Cui, G.C. Hadjipanayis, Effect of different surfactants on the formation and morphology of $SmCo_5$ nanoflakes. Acta Mater. **59**, 6772–6782 (2011). https://doi.org/10.1016/j.actamat.2011.07.035
26. M.J. Lucis, T. Prost, X. Jiang, M. Wang, J.E. Shield, Phase transitions in mechanically milled Mn-Al-C permanent magnets. Metals **4**, 130–140 (2014). https://doi.org/10.3390/met4020130
27. Q. Zeng, I. Baker, Z.-C. Yan, Nanostructured Mn–Al permanent magnets produced by mechanical milling. J. Appl. Phys. **99**, 08E902 (2006). https://doi.org/10.1063/1.2159187
28. O. Obi, L. Burns, Y. Chen, T. Fitchorov, S. Kim, K. Hsu, D. Heiman, L.H. Lewis, V.G. Harris, Magnetic and structural properties of heat-treated high-moment mechanically alloyed MnAlC powders. J. Alloys Compd. **582**, 598–602 (2014). https://doi.org/10.1016/j.jallcom.2013.08.086
29. G.B. Harris, Quantitative measurement of preferred orientation in rolled uranium bars. Philos. Mag. **43**, 113–123 (1952). https://doi.org/10.1080/14786440108520972
30. P.H. Zhou, L.J. Deng, J.L. Xie, D.F. Liang, Effects of particle morphology and crystal structure on the microwave properties of flake-like nanocrystalline Fe_3Co_2 particles. J. Alloys Compd. **448**, 303–307 (2008). https://doi.org/10.1016/j.jallcom.2006.10.061
31. X. Xiao, Z. Zeng, Z. Zhao, S. Xiao, Flaking behavior and microstructure evolution of nickel and copper powder during mechanical milling in liquid environment. Mater. Sci. Eng. A **475**, 166–171 (2008). https://doi.org/10.1016/j.msea.2007.04.084
32. A. Pasko, M. LoBue, E. Fazakas, L.K. Varga, F. Mazaleyrat, Spark plasma sintering of Mn–Al–C hard magnets. J. Phys. Condens. Matter **29**, 064203 (2014). https://doi.org/10.1088/0953-8984/26/6/064203